DFT/TDDFT Studies on the Electronic Structures and Spectral Properties of Rhenium(I) Pyridinybenzoimidazole Complexes

Xiaona Li,[†,‡] Xiaojuan Liu, Zhijian Wu, and Hongjie Zhang*,[†]

State Key Laboratory of Rare Earth Resource Utilizations, Changchun Institute of Applied Chemistry, Chinese Academy of Sciences, Changchun 130022, People's Republic of China, and Graduate School of the Chinese Academy of Sciences, Beijing, People's Republic of China

Received: July 1, 2008; Revised Manuscript Received: August 21, 2008

The electronic structures and spectral properties of three Re(I) complexes [$Re(CO)_3XL$] (X = Br, Cl; L = 1-(4−5′-phenyl-1,3,4-oxadiazolylbenzyl)-2-pyridinylbenzoimidazole (**1**), 1-(4-carbazolylbutyl)-2-pyridinylbenzoimidazole (**2**), and 2-(1-ethylbenzimidazol-2-yl)pyridine (**3**)) were investigated theoretically. The ground and the lowest lying triplet excited states were fully optimized at the B3LYP/LANL2DZ and CIS/LANL2DZ levels, respectively. TDDFT/PCM calculations have been employed to predict the absorption and emission spectra starting from the ground and excited state geometries, respectively. The lowest lying absorptions were calculated to be at 481, 493, and 486 nm for **1**−**3**, respectively, and all have the transition configuration of HOMO→LUMO. The lowest lying transitions can be assigned as metal/ligand-to-ligand charge transfer (MLCT/LLCT) character for **1**, ligand-to-ligand charge transfer (LLCT) character for **2**, and mixed MLCT/LLCT and intraligand $\pi\rightarrow\pi^*$ charge transfer (ILCT) character for **3**. The emission of **1** at 551 nm has the ^{3}MLCT/^{3}LLCT character, **2** has the ^{3}MLCT/^{3}LLCT character at 675 nm, and the 651nm transition of **3** has the character of ^{3}MLCT/^{3}LLCT/^{3}ILCT. Ionization potentials (IP) and electron affinities (EA) calculations show that the comparable EA and smaller IP values and the relativly balanceable charges transfer abilitie of **2** with respect to **1** and **3** result in the higher efficiency of OLEDs. The calculated results show that the absorption and emission transition character and device's efficiency can be changed by altering the ancillary ligands.

1. Introduction

Recently, the research of electroluminescent materials has been the subject of interest since the pioneering work done by Tang and VanSlyke, who first used tris(8-hydroxyquinoline)aluminum (Alq_3) to fabricate organic light-emitting diodes (OLED).[1] Nowadays, some researchers have extended their attention to heavy metal-coordinate complexes, even rare-earth complexes containing Tb(III)[2] and Eu(III)[3] ions, and recently our group reported the electroluminescent rare-earth complexes containing Dy[4] and Sm.[5] However, a major drawback of low extinction coefficients and efficient luminescence quenching limits their application for fabricating OLED. The phosphorescent transition metal complexes such as Os(II),[6] Ru(II),[7] Pt(II),[8] and Ir(III)[9] species have been extensively investigated over the past few decades. Many of these complexes possess an octahedral d^6 electron configuration, which is often adaptable for luminescent sensor design because of the presence of high extinction coefficients, as a result of metal-to-ligand charge transfer (MLCT). Due to the strong spin−orbit coupling resulting from heavy metal, these complexes can display molecular phosphorescence. Theoretically, the devices prepared by using phosphorescent heavy metal complexes would display efficiency 3−4 times better than that of devices based on fluorescent materials.[10]

With the aim of further extending the scope, great efforts have been focused on rhenium(I) analogues. A great number of rhenium(I) tricarbonyl diimine complexes have been extensively studied for their photophysical properties, solar energy conversion, OLED, and potential applications on the basis of their emission character.[11] Generally, these Re(I) complexes have broad and structureless emission bands that are sensitive to the change of the environments, such as by varying the ancillary ligand with electron-donating or electron-withdrawing ones. Therefore, the modification of ligand structure of these complexes can result in subtle tuning of their structural, photophysical, and luminescent characteristics. For example, replacement of X (ancillary ligand) in (X_2-bipyridine)$Re^I(CO)_3Cl$ complexes with different π-conjugated species can significantly change the energy gap between the highest occupied molecular orbital (HOMO) and the lowest unoccupied molecular orbital (LUMO) and the spectral properties of these complexes.[11g] Rillema and co-workers have reported the preparation and photophysical properties of a series of $[Re(CO)_3(CN_x)(L)]^+$ complexes, where L = 1,10-phenanthroline ramifications and (CN_x) = 2,6-dimethylphenylise cyanide ligand. The computational results reveal that the lowest lying emitting states can be tuned from metal−ligand-to-ligand charge transfer (^{3}MLLCT) to the ligand-centered (^{3}LC) state by varying the ancillary ligand.[12]

Very recently, a series of Re^I-diimine complexes $Re^I(CO)_3XL$ (X = Br, Cl; L = 1-(4-5′-phenyl-1,3,4-oxadiazolylbenzyl)-2-pyridinylbenzoimidazole (pob-pybm), 1-(4-carbazolylbutyl)-2-pyridinylbenzoimidazole (cb-pybm), 2-(1-ethylbenzimidazol-2-yl)pyridine (ethyl-pybm)) have been synthesized by Li,[13] Huang,[14] and co-workers, respectively. The electrophosphorescent devices were fabricated by doping these complexes as emitters. Li[13] concluded that the introduction of the carbazole

* Corresponding author. Phone: +86 431 85262127. Fax: +86 431 85698041. E-mail: hongjie@ciac.jl.cn (H.-J. Zhang).
† Chinese Academy of Sciences.
‡ Graduate School of the Chinese Academy of Sciences.

10.1021/jp805758n CCC: $40.75
Published on Web 10/15/2008

group into the pybm moiety improves the performance of the device with the maximum brightness of 2300 cd/cm^2 at 16 V. The structure, absorption, and emission spectra of the complexes were measured in dichloromethane (CH_2Cl_2) media. Complexes **1** and **2** in CH_2Cl_2 solution and **3** in $CHCl_3$ solution show luminescence of 590, 570, and 606 nm, respectively, and the observed emissions of **1**−**3** have been attributed to originate from MLCT excited states. Moreover, the spectroscopic properties and electron structures are crucial to gain insight into emission color change with different ancillary ligands. An understanding of the photochemistry properties of these complexes requires knowledge of molecular orbitals, spectra, and the appropriate excited state. Li[13] and Huang[14] have investigated the luminescent properties of these Re^I complexes, but they could not interpret the spectroscopic properties from an electronic structure point of view. Therefore, a detailed theoretical investigation of electronic structure and spectral properties of the above three complexes was undertaken in this work, using density functional theory (DFT) and time-dependent density functional theory (TDDFT). The aim of the theoretical investigation is 2-fold: (1) to establish how the electronic structures and spectral properties of **1**−**3** are influenced by different ancillary ligands and (2) to make a complete assignment of the UV/vis spectra with a special emphasis on the low-energy transitions responsible for the visible absorption, which are ascribed to the mixture of MLCT and ligand-to-ligand charge transfer (LLCT) as observed in experiments.[13,14] Then a significative indication can be obtained for future synthesizing and designing new luminescent materials with practical application perspective.

2. Computational Details

The geometrical structures of the singlet ground state (S_0) and the lowest lying triplet excited state (T_1) were optimized by the DFT[15] method with B3LYP functional[16] and the configuration interaction with single excitations (CIS)[17] approach, respectively. All geometrical structures were fully optimized without any symmetry constraints. On the basis of the optimized ground and excited state geometry structures, the absorption and emission spectra properties in dichloromethane (CH_2Cl_2) media were calculated by time-dependent functional theory (TDDFT)[18] approach associated with the polarized continuum model (PCM).[19] The TDDFT approach has been demonstrated to be reliable for calculating spectra properties of many transition metal complexes. [20] Due to the presence of electronic correlation in the TDDFT (B3LYP) method it can yield more accurate electronic excitation energies than the CIS method. Spin−orbital coupling is not included in the current TDDFT method and it influences the excitation energies for d(Re)-joined transitions suggested by Su and co-workers recently,[21] whereas it has a negligible effect on the transition character of these complexes. Hence, although TDDFT cannot exactly estimate the excitation energies for d(Re)-joined transitions, it can still provide a reasonable spectral feature for our investigated complexes.

In the calculation, the quasirelativistic pseudopotentials of Re atoms proposed by Hay and Wadt[22] with 14 valence electrons (outer-core [(5s^{2}5p^6)] electrons and the (5d^6) valence electrons) were employed, and a "double-ξ"quality basis set LANL2DZ, in which the Duning D95V basis set on the first row atoms, Los Alamos ECP plus DZ on Na−Bi was adopted as the basis set. To precisely describe the molecular properties, one additional f-type polarization functional is implemented for the Re^I atom ($\alpha_f = 2.033$).[23] The 6-31G(d)[24] basis set was employed on C, H, N, O, Br, and Cl atoms, respectively, for the ground and the lowest lying triplet excited state geometries optimization. In addition, the positive and negative ions with regard to the "electron-hole" creation are relevant to their use as OLED materials. Thus, ionization potentials (IP), electron affinities (EA), and reorganization energy (λ) were obtained by comparing the energy levels of neutral molecule with positive ions and negative ions, respectively. The calculated electronic density plots for frontier molecular orbitals were prepared by using the GaussView 3.07 software. All the calculations were performed with the Gaussian 03 software package[25] on an Origin/3900 server.

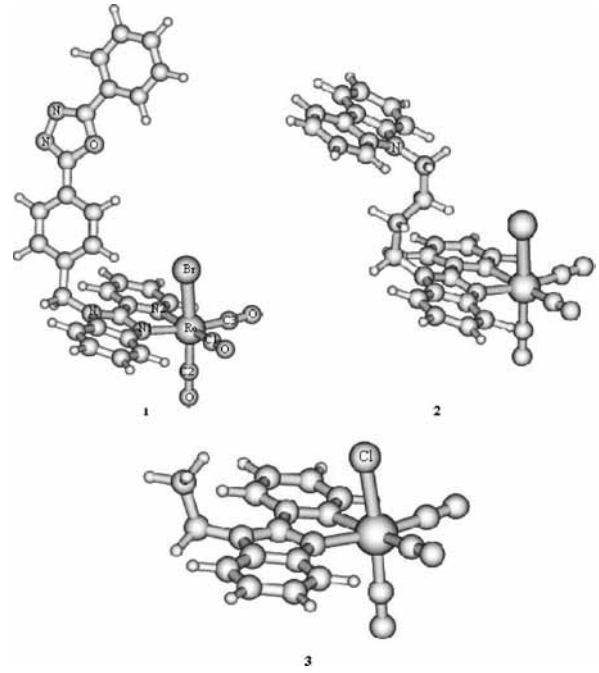

Figure 1. Optimized gound state geometrical structures of [Re(CO)$_3$LBr] [L = pob-pybm (**1**), cb-pybm (**2**)] and [Re(CO)$_3$LCl] [L = ethyl-pybm (**3**)] at the B3LYP/LANL2DZ level.

TABLE 1: Selected Optimized Geometrical Parameters of 1−3 in the Ground and Lower Lying Triplet Excited States at the B3LYP and CIS Levels, Respectively, Together with the Crystal Data of 2[13]

	1		**2**		**3**		
	S_0	T_1	S_0	T_1	S_0	T_1	exptl[12]
bond length (Å)							
Re−C1	1.927	1.963	1.927	1.963	1.925	1.962	1.863(13)
Re−C2	1.918	1.945	1.918	1.948	1.920	1.948	1.994(11)
Re−C3	1.928	1.965	1.926	1.976	1.927	1.975	1.904(11)
Re−Br(C1)	2.682	2.708	2.679	2.709	2.524	2.553	2.592(12)
Re−N1	2.187	2.218	2.196	2.191	2.187	2.192	2.149(17)
Re−N2	2.223	2.270	2.223	2.256	2.226	2.250	2.195(18)
bond angle (deg)							
C1−Re−C3	89.8	89.6	89.8	89.8	89.7	89.3	90.0(5)
N1−Re−N2	73.4	72.1	73.3	73.6	73.3	73.7	72.7(3)
Br−Re−C1	91.1	90.2	91.5	89.6	91.5	90.1	88.2(4)
Br−Re−C2	176.2	175.5	176.3	176.8	175.8	175.9	178.4(3)

3. Results and Discussion

3.1. The Ground State Geometries. The optimized ground state geometrical structures of **1**, **2**, and **3** in the gas phase at the B3LYP/LANL2DZ level are shown in Figure 1. Selected bond lengths and angles are summarized in Table 1 and the corresponding crystal data of **2** obtained from experiment[13] are also given. The calculated results revealed that the ground state

TABLE 2: Frontier Molecular Orbital Compositions (%) in the Ground State for Complex [Re(CO)$_3$pobBr] (1) at the B3LYP/LANL2DZ Level

			contribution (%)				
orbital	energy (eV)	bond type	Re	CO	Br	pybm	pob
163a	−0.7557	π*(pob) + π*(pybm)				14.3	85.1
162a	−1.0452	π*(pob)					98.7
161a	−1.7094	π*(pybm) + π*(pob)				85.9	11.6
160a	−1.8977	π*(pybm) + π*(pob)				16.5	83.1
159a	−2.6646	π*(pybm)				88.1	
HOMO−LUMO gap (2.87 eV)							
158a	−5.5313	d(Re) + π(CO) + π(Br)	$7.0d_{xy} + 9.0d_{yz} + 6.8d_{z^2}$	12.7	43.0		
157a	−5.6287	d(Re) + π(CO) + π(Br)	$5.7d_{xz} + 6.9d_{x^2-y^2} + 6.5d_{z^2}$	10.6	44.7		
156a	−6.3259	π(pob)					92.1
155a	−6.3373	d(Re) + π(CO) + π(pob) + π(Br)	$7.3d_{xy} + 23.9d_{xz} + 11.2d_{z^2}$	18.3	6.7		27.9
154a	−6.4045	d(Re) + π(CO) + π(Br) + π(pybm)	$3.9d_{xz} + 2.6d_{x^2-y^2}$	6.9	26.1		24.6

TABLE 3: Frontier Molecular Orbital Compositions (%) in the Ground State for Complex [Re(CO)$_3$cbBr] (2) at the the B3LYP/LANL2DZ Level

			contribution (%)				
orbital	energy (eV)	bond type	Re	CO	Br	pybm	cb
160a	−0.6629	π*(pybm) + d(Re)		11.8		84.1	
159a	−0.8128	π*(cb)					98.8
158a	−1.8292	π*(pybm)				92.1	
157a	−2.6787	π*(pybm)				82.4	
HOMO−LUMO gap (2.79 eV)							
156a	−5.4671	π(cb)	$0.9d_{xy} + 0.2d_{x^2-y^2}$				93.7
155a	−5.5389	d(Re) + π(CO) + π(Br) + π(cb)	$12.3d_{xz} + 10.6d_{z^2}$	12.9	41.9		17.6
154a	−5.6393	d(Re) + π(CO) + π(Br) + π(cb)	$16.5d_{xy} + 3.1d_{x^2-y^2}$	10.2	41.1		21.6
153a	−5.8440	π(cb)					98.0
152a	−6.3447	d(Re) + π(CO) + π(cb)	$3.5d_{xy} + 7.3d_{yz} + 32.2d_{x^2-y^2}$	19.6			27.3

geometries of the three complexes display a distorted octahedral arrangement of ligands around the metal center because these complexes have similar geometrical structures with the only differences being in the ancillary ligands connected to the peripheral nitrogen atom of the pybm moiety. A bromine (or chlorine) atom and one carbonyl group occupy the axial positions and coordinate with the center metal linearly as indicated from the calculated Br (or Cl)−Re−C2 angles around 176°. The other two carbonyl groups along with two nitrogen atoms in the pybm moiety occupy the equatorial positions. The optimized bond lengths and angles found can be roughly reproduced by the crystal data of **2**[13] except that the axial Re−Br (or Cl) bond lengths are overestimated. This is consistent with the research of other groups.[26] In addition, it is worth noting that the Re−C1 and Re−C3 bond lengths in the equatorial positions are always longer than that of Re−C2 in the axial position. This is attributed to the different ligand→to→metal back-bonding abilities at the axial and the equatorial positions. It is well-known that the nature of the metal−ligand bond can be described as a donation from a σ orbital of the ligand toward an empty d orbital of the metal and a concurrent back-donation from a filled d orbital to a π* antibonding orbital of the ligand. Because the bromine group has stronger electron donation ability to the metal d orbital than the equatorial N atoms, the axial carbonyl group benefits more from the increased back-bonding and gives rise to a shorter and stronger Re−C2 bond length. The Re−C2 bond length in **3** is slightly longer than that in **1** and **2** because chlorine is a weaker electron donator compared with bromine. Generally, the calculated bond lengths are longer than the experimental data because the former are optimized in the gas phase and the latter are in a tight crystal lattice.

3.2. Frontier Molecular Orbital Properties. Since the observed differences in the optical and chemical properties of these complexes rely mainly on the changes in the ground state electronic structure, we will discuss in detail the ground state electronic structure of these complexes with a special emphasis on the frontier molecular orbitals components, the HOMO and LUMO energy levels, and energy gaps. The frontier molecular orbital compositions and energy levels of **1**−**3** are shown in Tables 2−4 and Figure 2, respectively. The assignment of the type of each MO was made on the basis of its composition and by visual inspection of its three-dimensional representation.

As shown in Table 2, the HOMO of **1** is mainly composed of Re d orbital ($9.0\%d_{yz} + 7.0\%d_{xz} + 6.8\%d_{z^2}$), carbonyl group (12.7%), and bromine group (43.0%). For **3**, the Re d orbital ($19.7\%d_{yz} + 8.0\%d_{xz}$), carbonyl group (15.8%), chlorine group (31.9%), and pybm moiety (20.4%) contribute the composition as shown in Table 4 and Figure 2. It is obvious in Figure 2 that in the HOMO the Re d orbital is antibonding with the axial bromine group, while it is bonding with the three carbonyl groups as shown by the appreciable electron density on the carbon and bromine atoms for **1** and **3**. The ancillary ligands do not play a significant role on the composition of HOMO for **1** and **3**. But with respect to **2**, however, the HOMO is essentially a π orbital on the carbazole group and is localized predominantly on the nitrogen atom and the π-conjugated aryl ring. As shown in Figure 2, the nitrogen atom is π-antibonding with respect to the two carbon atoms of the aryl ring. There is little composition of the Re d orbital since there is no Re dπ contribution. This conclusion is consistent with the calculation of *fac*-$[Re(CO)_3(CN_x)(L)]^+$ complexes obtained by Rillema in which the composition in HOMO is exclusively localized on the (CN_x) ligand in which the ligand is pyrrole.[12] The composition of the LUMO of **1**−**3** is a π* orbital localized on the pybm moiety with more than 80% composition, showing that the ancillary ligands do not cause a significant change in LUMO distribution. But the ancillary ligands can tune the distribution of the HOMO orbital. This distribution will result in different electronic transition character upon excitation. For other lower occupied and higher virtual frontier MOs, the ancillary ligands

TABLE 4: Frontier Molecular Orbital Compositions (%) in the Ground State for Complex [Re(CO)$_3$EthylCl] (3) at the B3LYP/LANL2DZ Level

			contribution (%)				
orbital	energy (eV)	bond type	Re	CO	Cl	pybm	ethyl
99a	−0.5712	π*(pybm)				83.4	
98a	−1.7228	π*(pybm)				93.5	
97a	−2.5949	π*(pybm)				91.1	
HOMO−LUMO gap (2.86 eV)							
96a	−5.4532	d(Re) + π(CO) + π(Cl) + π(pybm)	19.7d_{yz} + 8.0d_{xz}	15.8	31.9	20.4	
95a	−5.5577	d(Re) + π(CO) + π(Cl) + π(pybm)	3.6d_{xy} + 7.8d_{yz} + 15.2d_{xz}	13.5	35.5	21.6	
94a	−6.2200	d(Re) + π(CO) + π(pybm)	43.7d_{z^2}	20.9		29.9	
93a	−6.4886	d(Re) + π(Cl) + π(pybm)	6.3d_{yz}		28.5	48.9	
92a	−6.7419	d(Re) + π(Cl) + π(pybm)	11.9d_{xz}		30.5		48.1

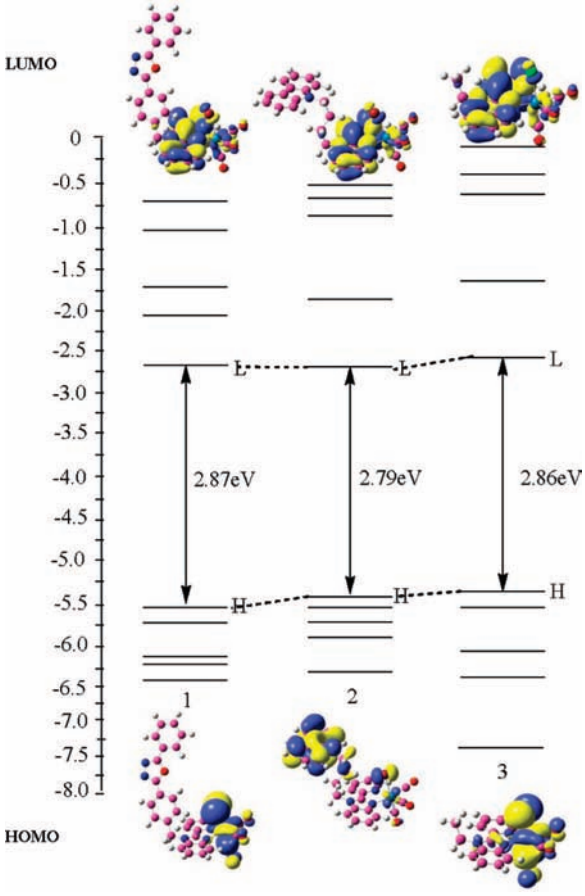

Figure 2. Pictorial representation of the frontier molecular orbital energy levels of the three complexes calculated in the gas phase at the B3LYP/LANL2DZ level. In addition, the electron density plots of the highest occupied molecular orbital (HOMO) and the lowest unoccupied molecular orbital (LUMO) of **1**−**3** are also presented.

have a significant role in controlling the compositions of **1** and **2**. For **1**, HOMO-2 (156a), LUMO+1 (160a), LUMO+3 (162a), and LUMO+4 (163a) are mainly composed of the ancillary ligand (more than 80%). For **2**, the π orbital in HOMO-3 (153a) and the π* orbital in LUMO+2 (159a) are calculated to be almost exclusively located on the carbazole group. But with respect to **3**, there is no obvious composition found located on the ethyl group.

Moreover, the orbital energy levels of HOMO and LUMO are influenced by changing the ancillary ligands. As shown in Figure 2, the stabilization of the HOMO level is more prominent in **1** than that of **2** and **3**, and the order of stabilization of the HOMO energy levels is as follows: **1** (−5.53 eV) > **2** (−5.47 eV) > **3**(−5.45 eV), which is consistent with the order of introduction of the increased π-conjugation groups in the order **1** > **2** > **3**. The carbazole group itself is a good π-conjugation unit, but the alkyl group between the carbazole group and the (pybm)Re(CO)$_3$Br moiety destroys the extending of π-conjugation and dramatically decreases the electron delocalization within the whole ligand, therefore, destabilizing the HOMO energy level compared with **1**. This raised HOMO energy level of **2** by the integration of a carbazole unit to the pybm moiety will benefit the hole-transporting ability in the resulting complex relative to complex **1**. The same conclusion has been obtained for some Ir complexes containing the carbazole unit,[27] in which the inclusion of the carbazole group is favorable for hole-transporting properties. The LUMO energy level of **1** (−2.66 eV) is comparable to that of **2** (−2.68 eV) with only 0.02 eV destabilization, which results in the broader HOMO−LUMO gap in **1** (2.87 eV) than in **2** (2.79 eV). This indicates that the effect of the carbazole group on the energy of the π* orbital is negligible, which is consistent with the experimental observation that the photoluminescence spectra of (pybm)Re(CO)$_3$Br and **2** are similar due to the longer distance between the carbazole ligand and the pybm moiety.[13] The HOMO−LUMO gap of **2** is also smaller than that of **3** (2.86 eV) due to the comparable HOMO energy level and higher LUMO level in **3**. The lower HOMO energy levels of **1** and **2** will ensure the efficient hole injection abilities and the slight increase of the LUMO levels would not worsen the electron injection ability of **1** compared with **2**, while with respect to **3**, it will have a comparable hole injection ability to **2**, while the higher LUMO energy level will significantly lower the electron injection ability.[28]

3.3. Absorption Spectra. The absorption spectra in CH_2Cl_2 solution for **1**−**3** were explored at the TDDFT/B3LYP level. The polarized continuum model (PCM) in SCRF is used in which the solvent is simulated as a continuum of uniform dielectric constant ϵ. The calculated absorption spectra associated with their oscillator strengths, assignment, configurations, excitation energies, and excitations with maximum CI coefficients are listed in Table 5. For clarity, only the most leading excited states (with larger CI coefficients) are listed. The fitted absorption curve for **1**−**3** as oscillator strength vs wavelength is depicted in Figure 3.

As shown in Table 5, the lowest lying singlet → singlet absorptions of **1**−**3** are calculated at 481, 493, and 486 nm, respectively. The lowest lying singlet → singlet absorption of **1** is blue-shifted compare to those of **2** and **3**, and **3** is again blue-shifted compared with that of **2**, which is consistent with the variation rules of the HOMO−LUMO energies gaps. This blue shift of the shorter wavelength band is attributed to the intense participation of the carbazole group in **2**, which stabilized the molecular orbital compared with **1** and **3**. The configurations of HOMO→LUMO are responsible for the lowest lying transitions of the three complexes, especially for **1**, which is a pure

TABLE 5: Absorptions of 1−3 in Dichloromethane (CH_2Cl_2) Solution According to TDDFT (B3LYP) Calculations

complex	transition	(CI coeff)	E (eV)/(nm)	oscillator	assign	λ_{exp}(nm)
1	$S_1$158a → 159a	0.70199(100%)	2.58/481	0.0001	MLCT/LLCT/ILCT	420[a]
	$S_2$155a → 159a	0.52477(100%)	3.42/363	0.0604	MLCT/LLCT	
	$S_8$156a → 160a	0.50949 (55%)	3.67/338	0.0628	ILCT/LLCT	340[a]
	153a → 159a	0.38607(31%)			MLCT/LLCT	
	S_{12}156a → 160a	0.64629(94%)	4.01/309	0.9870	ILCT/LLCT	284[a]
2	$S_1$156a → 157a	0.69390(98%)	2.52/493	0.0064	LLCT	
	$S_6$152a → 157a	0.50870(57%)	3.42/362	0.0549	MLCT/LLCT	366[a]
	151a → 157a	0.39888(35%)			MLCT/LLCT/ILCT	
	S_{11}150a → 157a	−0.46294(49%)	3.81/325	0.2822	MLCT/LLCT	328[a]
	148a → 157a	0.43919(44%)			ILCT/LLCT	
3	S_1 96a → 97a	0.68973(97%)	2.55/486	0.0022	MLCT/LLCT/ILCT	
	S_5 93a → 97a	0.53758(64%)	3.57/347	0.0672	MLCT/LLCT/ILCT	347[b]
	96a → 98a	0.30348(22%)			MLCT/LLCT/ILCT	
	S_7 92a → 97a	0.57908(74%)	3.77/329	0.3184	MLCT/LLCT/ILCT	331[b]

[a] From ref 13. [b] From ref 14.

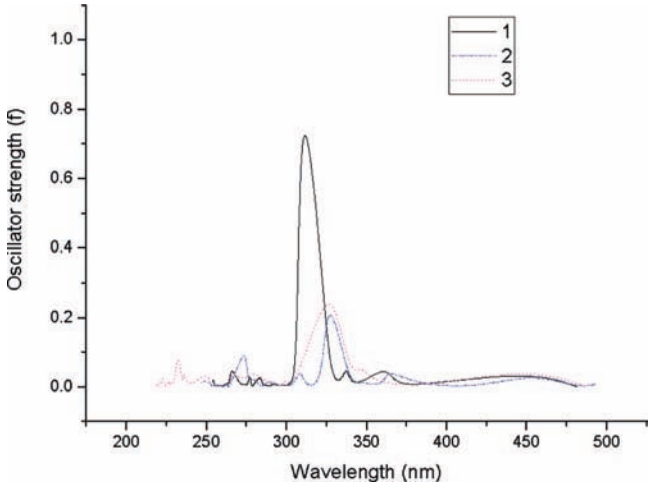

Figure 3. The simulated absorption spectra of complexes **1**−**3** at the TDDFT (B3LYP)/LANL2DZ level in dichloromethane media.

HOMO→LUMO transition. Table 2 shows that the HOMO (158a) of **1** is mainly composed of ca. 22.8% metal Re^I d orbital ($7.0\%d_{xy} + 9.0\%d_{yz} + 6.8\%d_{z^2}$), 12.7% carbonyl group, and 43.0% bromine group. The LUMO (159a) of **1** is a π^*(pybm) type orbital. Thus, the transition at 481 nm for **1** can be described as a [d(Re) + π(CO) + π(Br)] → [π^*(pybm)] transition with MLCT/LLCT character. For **3**, as shown in Table 4, the composition of HOMO (96a) is similar to that of **1** but the proportion on pybm moiety increased to 20.4%. The lowest lying transition of **3** at 486 nm is attributed to a [d(Re) + π(CO) + π(Cl) + π(pybm)] → [π^*(pybm)] transition with the character of MLCT/LLCT/ILCT. With respect to **2**, the HOMO (156a) is a π(cb) type orbital and the LUMO is a π^*(pybm) type orbital, thus the 493 nm transition can be described as LLCT character ([π(cb) → π^*(pybm)]).

The first distinguished lower energy absorption bands appear at 344−377nm for **1**, 358−386 nm for **2**, and 341−360 nm for **3** and the transitions with the largest oscillator strengths localized at 363, 362, and 347 nm dominant these low-energy absorption bands for **1**−**3**, respectively. For **2** and **3**, the calculated 362 and 347 nm absorption bonds correspond to the 366 and 347 nm absorptions in experiments, respectively.[13,14] As shown in Tables 2−4 and 5, the transition of 155a → 159a of **1** at 363 nm can be described as [d(Re) + π(CO) + π(pob) + π(Br)] → [π^*(pybm)] with the transition character of MLCT and LLCT. Absorption of 362 nm for **2** is also a mixed transition character of MLCT and LLCT similar to that for **1** but with different metal composition. Transition of 151a[d(Re) + π(CO) + π(Br) + π(pybm)] → 157a[π^*(pybm)] also contributes to this lower energy absorption band of **2** with the mixed character of MLCT, LLCT, and ILCT. For **3**, the transition of 93a[d(Re) + π(Cl) + π(pybm)] → 97a[π^*(pybm)] (MLCT/LLCT/ILCT) dominates the absorption at 347 nm with a little contribution coming from 96a[d(Re) + π(CO) + π(Cl) + π(pybm)] → 98a[π^*(pybm)] (MLCT/LLCT/ILCT).

The experimentally observed strongest absorptions localized at higher energy regions are 284, 328, and 331nm for **1**−**3,** respectively. The calculated results in CH_2Cl_2 solution are 309, 325, and 329 nm for **1**−**3**, respectively. The calculated values of 325 (**2**) and 329 nm (**3**) are in good agreement with the experimental values of 328 and 331 nm, respectively. The dominant character within these higher energy absorptions is ILCT and/or LLCT, which is partly perturbed by the MLCT components. For **1**, the excitation of 152a(HOMO-2) → 160a(LUMO+1) contributes more than 94% of the transition, and both orbitals are nearly pure ancillary ligand character, thus the transition is attributed to ILCT. The MLCT component remarkably increases in **2** and the combined characters of MLCT and LLCT dominate the transition in **3**. The absorptions at λ < 300 nm are weaker and can be considered as intraligand π → π^* transitions which can be supported from the free ligand absorption spectra as shown in Figures S1−S3 in the Supporting Information.

The calculated results agree with the experimental observations that the MLCT component is more remarkable in the lower energy region. This is due to the presence of heavy metal effects involved in these complexes which can produce lower energy absorptions. Though the absorption of MLCT is weak, the participation of metals in these complexes probably makes the transition occur and therefore enhances the luminescence quantum yields. Moreover, different ancillary ligands can cause different excitation energy and transition character. Therefore, the modification of ligand structure can tune the photophysical and luminescent characteristics.

3.4. Ionization Potentials (IP) and Electron Affinities (EA). The device performance of OLEDs depends on the charge injection, transfer, and balance as well as the exciton confinement in a device. In this section, we present ionization potentials (IP), electron affinities (EA), and reorganization energy (λ) calculated for **1**, **2**, **3**, (pybm)$Re(CO)_3Br$, pob, and cb, together with hole extraction potential (HEP, an expression of IP) and electron extraction potential (EEP, an expression of EA). The IP and EA can be either for vertical excitations (v; at the geometry of neutral molecule) or adiabatic excitations (a; optimized structure for both the neutral and charged molecule).

TABLE 6: Ionization Potentials, Electronic Affinities, Extraction Potentials and Reorganization Energies for Each Molecule (in eV) Calculated at the DFT/B3LYP Level

molecule	IP(v)	IP(a)	HEP	EA(v)	EA(a)	EEP	λ_{hole}	$\lambda_{electron}$
1	8.79	6.76	6.95	1.35	1.52	1.54	1.84	0.19
2	6.65	6.59	6.67	1.31	1.53	1.54	−0.02	0.23
3	7.07	6.79	8.15	1.19	1.36	1.38	−1.08	0.19
(pybm)Re(CO)$_3$Br	7.54	6.82	6.72	1.36	1.41	1.53	0.82	0.17
pob	7.15	7.36	7.48	0.06	0.21	0.21	−0.33	0.15
cb	6.89	6.84	6.84	−1.0	−0.86	−0.85	−0.05	−0.15

TABLE 7: Phosphorescent Emissions of 1−3 in Dichloromethane Solution under the TDDFT Calculations, Together with the Experimental Values

	excitation	E_{cal}/(eV)	λ_{cal}	character	λ_{exp}
1	160a → 156a	2.2492	551.25	Re/Br/CO→pob (MLCT/LLCT)	601[a]
2	157a →155a	1.8361	675.34	cb→pybm (LLCT)	577[a]
	157a →151a			Re/CO/cb→pybm (MLCT/LLCT)	
3	97a →96a	1.9033	651.41	Re/pybm/Br/CO→Pybm(MLCT/LLCT/ILCT)	606[b]
	97a→ 93a			Re/CO→pybm(MLCT/LLCT)	

[a] From ref 13. [b] from ref 14.

In the experiment, oxidation potential E^{ox} and reduction potential E^{red} examined by cyclic voltammetry have a linear relationship to the energy levels: HOMO = $-(E^{ox} + 4.71)$ eV and LUMO = $-(E^{red} + 4.71)$ eV.[29] E^{ox} can be viewed as the energy required after losing an electron from the metal d orbital, while the E^{red} is the energy released after gaining an electron. For complexes with similar structures, the higher HOMO and lower LUMO energy levels will facilitate the hole- and electron-transporting abilities,[30] respectively. Ionization potentials (IP) and electron affinities (EA) have similar definitions of E^{ox} and E^{red}, respectively,[31] and have been demonstrated to have a similar linear relationship to the energy levels of the HOMO and LUMO.[32] Therefore, the IP and EA are used to evaluate the energy barrier for the injection of holes and electrons, and the reorganization energy is used to value the charge transfer (or transport) rate and balance.

As presented in Table 6, with respect to the VIP and VEA values, among carbazole, 2,5-diphenyl-1,3,4-oxadiazole, and complex (pybm)Re(CO)$_3$Br, ligand carbazole has the smallest IP value (6.89 eV) and (pybm)Re(CO)$_3$Br has the largest EA value (1.36 eV). The calculated results reveal that carbazole can act as a good hole-transporting group[27,33] and complex (pybm)Re(CO)$_3$Br has a greater electron-transporting ability. Thus, when (pybm)Re(CO)$_3$Br is linked with the hole-transporting group of carbazole, the hole or electron injection abilities will be improved with the smaller IP value of 6.65 eV and comparable EA value of 1.31 eV with respect to complex (pybm)Re(CO)$_3$Br, and we expect the effective carrier recombination of complex **2**. On the other hand, the introduction of a 2,5-diphenyl-1.3,4-oxadiazole group into (pybm)Re(CO)$_3$Br significantly enhances the IP value of complex **1** (up to 8.79 eV), and lowers the device's efficiency. The calculated results are consistent with the experimental observation that the order of the maximum efficiency of the OLED is as follows: complex **2** > (pybm)Re(CO)$_3$Br > complex **1**. For complex **3**, it has the favorable IP value, while the EA values are too small compared with **1** and **2**, which will enhance the hole-transporting ability and lower the electron-transporting ability, resulting in an unbalanced charge transport, and enhance nonradiative recombination because of interactions of excitons with the charge carries.[31] The calculated AIP and AEA values have generally the same trend to VIP and VEA. Moreover, the variation trend of IP and EA is in accord with the analysis from the HOMO and LUMO energies.

According to the Marcus/Hush model,[34−36] the charge (hole or electron) transfer rate k can be expressed by the following formula:

$$k = \left(\frac{\pi}{\lambda k_b T}\right)^{1/2} \frac{V^2}{\hbar} \exp\left(-\frac{\lambda}{4k_b T}\right) = A \exp\left(-\frac{\lambda}{4k_b T}\right) \quad (1)$$

where T is the temperature, k_b is the Boltzmann constant, λ is the reorganization energy, and V is the coupling matrix element between the cation and molecules, which is dictated by the overlap of orbitals. Obviously, the reorganization energy in the charge transfer process is very important. As shown in Table 6, the λ_{hole} values for **2**, **3**, and pob are smaller than the $\lambda_{electron}$ values, which suggests that the hole transfer rate is better than the electron transfer rate, and the electron transfer rate of **2** is worse than that of **1** and **3**. While the difference between $\lambda_{electron}$ and λ_{hole} (0.25) for **2** is much smaller than that of **1** and **3**, which can greatly improve the charge transfer balance of **2**, thus further enhancing the device performance of OLEDs. The above analysis of the variation trend of the HOMO and LUMO, and the charge transfer rate of holes and electrons, suggests that the performance of OLED can be greatly influenced by the ancillary ligands. The calculated results presented earlier information that the device performance can be easily changed by modifying or tuning the substituents. And it is a key point toward the development of novel transition metal-containing materials of OLEDs.

3.5. The Lowest Lying Triplet Excited State and Phosphorescence Spectra. ***3.5.1. The Lowest Lying Triplet Excited State.*** The lowest lying triplet excited state geometries of **1**−**3** are optimized based on the calculated ground state geometries and selected geometrical parameters are also listed in Table 1. The calculated results reveal that all the Re−C, Re−N, and Re−Br (or Cl) bond lengths are relatively longer than that in the corresponding ground states. The calculated Re−C bond lengths in the excited states relax by about 0.03−0.05 Å, because structural changes accompany excitation as well as electron density changes in the excited states. On the basis of the analysis of frontier molecular orbitals above, the occupied MO of **1** and **3** are Re d orbital, CO, and Br based, and virtual MO are almost pybm based. Thus, in an excited state, an electron transfers from a molecular orbital that is Re d orbital, CO, and Br based to one that is largely pybm based. This results in a decrease in electron density at the metal, which decreases Re−CO back-

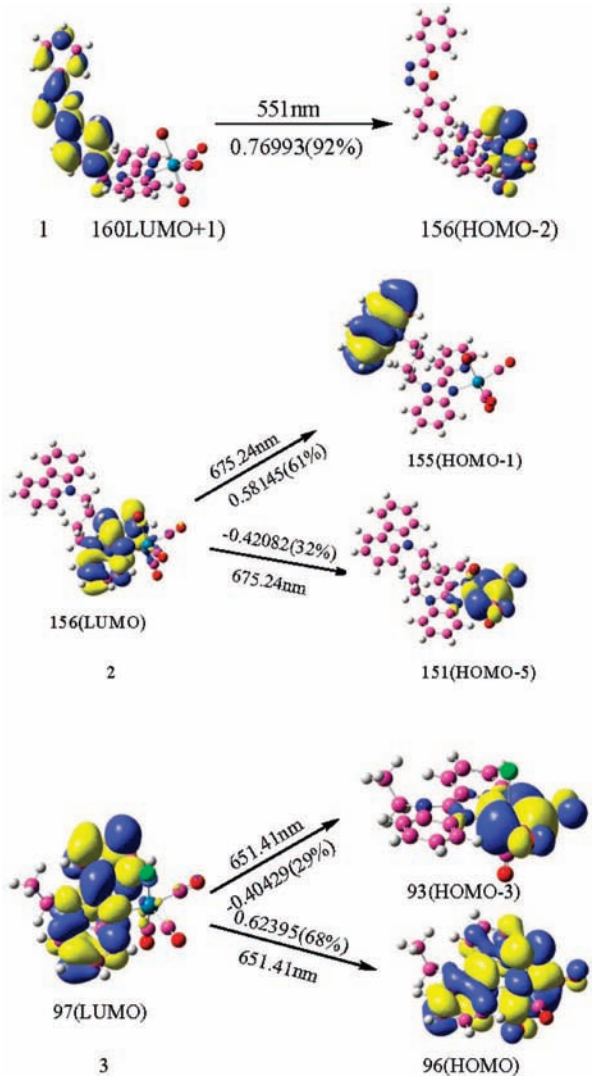

Figure 4. Single electron transitions for the emission at 551 nm for **1**, 675 nm for **2**, and 651 nm for **3**, respectively, in the TDDFT calculation in dichloromethane solution.

bonding and results in the weaker and longer Re−C bond lengths in the excited states. The bond angles of N1−Re−N2 and C1−Re−C3 are slightly larger compared with the ground state ones, while Br−Re−C1 bond angles are reduced by 1.9° and 1.4° for **2** and **3**, respectively, which are close to 90.0°. Br−Re−C2 bond angles increased 0.5° and 0.1° for **2** and **3**, respectively, indicating that the three atoms, Br (or Cl), Re, and C2, have the trend to be in the same line. The changes of bond angles indicate that the geometrical structures are closer to the octahedron upon excitation.

3.5.2. Phosphorescence Spectra. On the basis of the excited triplet state geometries optimized by the CIS method, the emission spectra of **1**−**3** in dichloromethane (CH_2Cl_2) solution are calculated at the TDDFT/B3LYP level associated with the PCM model. The results of the TDDFT calculations for **1**−**3** are listed in Table 7, associated with the emissive energies, transition assignments, and the experimental values. The plots of frontier molecular orbitals related to emissions of **1**−**3** are presented in Figure 4. To conveniently discuss the transition property of emission, we present the partial compositions of frontier molecular orbitals related to the emissions in Tables S1−S3 in the Supporting Information.

The calculated lowest energy emissions occur at 551 (2.2492 eV), 675 (1.8141 eV), and 651 nm (1.9033 eV) for **1**−**3**, respectively. For **1**, the emission at 551 nm is dominantly controlled by the excitation of 160a → 156a (CI 0.76993). As shown in Table S1 in the Supporting Information and Figure 4, 160 is a π*-type orbital localized on the pob moiety, while the d(Re) orbital (13.5%$d_{x^2-y^2}$ + 11.4%d_{yz} + 6.8%d_{z^2}), π(Br)(32.4%), and π(pob)(18.8%) contribute to the composition of 156a, thus the emission at 551 nm has the [π*(pob)] → [d(Re) + π(CO) + π(Br)] (^{3}MLCT/^{3}LLCT) transition character. With respect to the emission at 675 nm of **2**, the phosphorescence is mainly from the transitions of 157a (LUMO) → 155a (HOMO-1) (61%) and 157a (LUMO) → 151a (HOMO-5) (32%) configuration with a CI coefficient of 0.58145 and 0.42082, respectively. This emission has ^{3}MLCT [(π*(pybm) → π(cb)] and ^{3}MLCT/^{3}LLCT [π*(pybm) → d(Re) + π(CO) + π(cb)] character as shown in Figure 4 and Table S2 in the Supporting Information. Transitions of 97a (LUMO) → 96a (HOMO) (68%) and 97a (LUMO)→ 93a (HOMO-3) (29%) are in charge of the emission at 651 nm of **3**. For this emission, the electron transition in the luminescent process is mainly composed of [π*(pybm) → d(Re) + π(pybm) + π(Br) + π(CO)] (^{3}MLCT/^{3}LLCT/^{3}ILCT) and [π*(pybm) → d(Re) + π(CO) + π(pybm)] [^{3}MLCT/^{3}LLCT/^{3}ILCT]. Since the lowest energy emissions and absorptions have the same symmetry and transition character for each complex, the phosphorescent emissions should be the reverse process of the lowest energy absorptions.[31] We have presented here that the lowest energy absorptions of **1**−**3** arise from the MLCT/LLCT, LLCT, and MLCT/LLCT/ILCT transitions, respectively. Therefore, the calculated lowest energy phosphorescent emissions have the same transition character.

4. Conclusions

In this paper, we have applied DFT and TDDFT methods to investigate the geometry structures, absorptions, and phosphorescent properties of three Re(I) pyridinybenzoimidazole complexes. The calculated results reveal that the HOMO of **1** and **3** is mainly composed of the Re d orbital, carbonyl group, and bromine (or chlorine) group. But with respect to **2**, the HOMO is essentially a π orbital localized on the carbazole group. The LUMO of **1**−**3** is mainly localized on the pybm moiety. The lowest energy absorptions all have the transition configurations of HOMO→LUMO, therefore, results in the transition character of MLCT/LLCT, LLCT, and MLCT/LLCT/ILCT for **1**−**3**, respectively. The phosphorescence at 551 nm for complex **1** has [π*(pob)] → [d(Re) + π(CO) + π(Br)] (^{3}MLCT/^{3}LLCT) transition character, the main emission at 675 nm for **2** has the transition character of [π*(pybm) → (π(pob)]^{3}LLCT, and the main emission at 651 nm for **3** has the transition character of [π*(pybm) → d(Re) + π(CO)] ^{3}MLCT/^{3}LLCT/^{3}ILCT. The calculated ionization potentials (IP), electron affinities (EA), and reorganization energy (λ) indicate that with the incorporation of hole-transporting and electron-transporting groups into one molecule (**2**), the device performance will be improved due to the more balanceable charge transfer abilities. We hope these theoretical studies can provide constructive information in designing novel and high-efficiency OLED materials.

Acknowledgment. The authors are grateful to the financial aid from the National Natural Science Foundation of China (Grant Nos. 20490210, 20631040, 20602035, and 20771099) and the MOST of China (Grant Nos. 2006CB601103 and 2006DFA42610).

Supporting Information Available: Simulated absorption spectra of ligand **1** at the TDDFT (B3LYP)/LANL2DZ level

in dichloromethan media. This material is available free of charge via the Internet at http://pubs.acs.org.

References and Notes

(1) Tang, C. W.; VanSlyke, S. A. *Appl. Phys. Lett.* **1987**, *51*, 913.

(2) (a) Wang, J. F.; Wang, R. Y.; Yang, J.; Zheng, Z. P.; Carducci, M. D.; Cayou, T.; Peyghambarian, N.; Jabbour, G. E. *J. Am. Chem. Soc.* **2001**, *123*, 6179. (b) Christou, V.; Salata, O. V.; Ly, T. Q.; Capecchi, S.; Bailey, N. J.; Cowley, A.; Chippindale, A. M. *Synth. Met.* **2000**, *111*−*112*, 7. (c) Eliseeva, S.; Kotova, O.; Mirzov, O.; Anikin, K.; Lepnev, L.; Perevedentseva, E.; Vitukhnovsky, A.; Kuzmina, N. *Synth. Met.* **2004**, *141*, 225. (d) Kim, Y. K.; Pyo, S. W.; Choi, D. S.; Hue, H. S.; Lee, S. H.; Ha, Y. K.; Lee, H. S.; Kim, J. S.; Kim, W. Y. *Synth. Met.* **2000**, *111*−*112*, 113. (e) Xin, H.; Li, F. Y.; Shi, Mei.; Bian, Z. Q.; Huang, C. H. *J. Am. Chem. Soc.* **2003**, *125*, 7166.

(3) (a) Li, S. F.; Zhong, G. Y.; Zhu, W. H.; Li, F. Y.; Pan, J. F.; Huang, W.; Tian, H. *J. Mater. Chem.* **2005**, *15*, 3221. (b) Sun, P. P.; Duan, J. P.; Shih, H. T.; Cheng, C. H. *Appl. Phys. Lett.* **2002**, *81*, 792. (c) Yu, J. B.; Zhou, L.; Zhang, H. J.; Zheng, Y. X.; Li, H. R.; Deng, R. P.; Peng, Z. P.; Li, Z. F. *Inorg. Chem.* **2005**, *44*, 1611. (d) Adachi, C.; Baldo, M. A.; Forrest, S. R. *J. Appl. Phys.* **2000**, *87*, 8049.

(4) Li, Z. F.; Zhou, L.; Yu, J. B.; Zhang, H. J.; Deng, R. P.; Peng, Z. P.; Guo, Z. Y. *J. Phys. Chem. C* **2007**, *111*, 2295.

(5) Zheng, Y. X.; Fu, L. S.; Zhou, Y. H.; Yu, J. B.; Yu, Y. N.; Wang, S. B.; Zhang, H. J. *J. Mater. Chem.* **2002**, *12*, 919.

(6) Chen, Y. L.; Lee, S. W.; Chi, Y.; Hwang, K. C.; Kumar, S. B. *Inorg. Chem.* **2005**, *44*, 4287.

(7) Chan, W. K.; Ng, P. K.; Gong, X.; Hou, S. J. *Appl. Phys. Lett.* **1999**, *75*, 3920.

(8) Cho, J. Y.; Domercg, B.; Barlow, S.; Suponitsky, K. Y.; Li, J.; Timofeeva, T. V.; Jones, S. C.; Hayden, L. E.; Kimyonok, A.; South, C. R.; Weck, M.; Kippelen, B.; Marder, S. R. *Organometallics* **2007**, *26*, 4816.

(9) (a) Yu, X. M.; Kwok, H. S.; Wong, W. Y.; Zhou, G. J. *Chem. Mater.* **2006**, *18*, 5097. (b) Lamansky, S.; Djurovich, P.; Murphy, D.; Razzaq, F. A.; Lee, H. E.; Adachi, C.; Burrows, P. E.; Forrest, S. R.; Thompson, M. E. *J. Am. Chem. Soc.* **2001**, *123*, 4304. (c) Lamansky, S.; Djurovich, P.; Murphy, D.; Razzaq, F. A.; Kwong, R.; Tsyba, I.; Bortz, M.; Mui, B.; Bau, R.; Thompson, M. E. *Inorg. Chem.* **2001**, *40*, 1704.

(10) Adachi, C.; Baldo, M. A.; Forrest, S. R.; Thompson, M. E. *Appl. Phys. Lett.* **2000**, *77*, 904.

(11) (a) Lo, K. K. W.; Lau, J. S. Y.; Fong, V. W. Y. *Organometallics* **2004**, *23*, 1098. (b) Li, F.; Zhang, M.; Cheng, G.; Feng, J.; Zhao, Y.; Ma, Y. G.; Liu, S. Y.; Shen, J. C. *Appl. Phys. Lett.* **2004**, *84*, 148. (c) Chan, W. K.; Ng, P. K.; Gong, X.; Hou, S. J. *Appl. Phys. Lett.* **1999**, *75*, 3920. (d) Gong, X.; Ng, P. K.; Chan, W. K. *Adv. Mater.* **1998**, *10*, 1337. (e) Li, F.; Zhang, M.; Feng, J.; Cheng, G.; Wu, Z. J.; Ma, Y. G.; Liu, S. Y.; Sheng, J. C.; Lee, S. T. *Appl. Phys. Lett.* **2003**, *83*, 365. (f) Li, B.; Li, M. T.; Hong, Z. R.; Li, W. L.; Yu, T. Z.; Wei, H. Z. *Appl. Phys. Lett.* **2004**, *85*, 4786. (g) Walters, K. A.; Kim, Y. J.; Hupp, J. T. *Inorg. Chem.* **2002**, *41*, 2909. (h) Dunn, A. R.; Bittner, W. B.; Winkler, J. R.; Getzoff, E. D.; Stuehr, D. J.; Gray, H. B. *J. Am. Chem. Soc.* **2005**, *127*, 5169.

(12) Villegas, J. M.; Stoyanov, S. R.; Huang, W.; Rillema, D. P. *Inorg. Chem.* **2005**, *44*, 2297.

(13) Si, Z. J.; Li, J.; Li, B.; Zhao, F. F.; Liu, S. Y.; Li, W. L. *Inorg. Chem.* **2007**, *46*, 6155.

(14) Wang, K. Z.; Huang, L.; Gao, L. H.; Jin, L. P.; Huang, C. H. *Inorg. Chem.* **2002**, *41*, 3353.

(15) Runge, E.; Gross, E. K. U. *Phys. Rev. Lett.* **1984**, *52*, 997.

(16) Mayo, S. L.; Olafson, B. D.; Goddard, W. A., III *J. Phys. Chem.* **1990**, *94*, 8897.

(17) (a) Foresman, J. B.; Gordon, M. H.; Pople, J. A.; Frisch, M. J. *J. Phys. Chem.* **1992**, *96*, 135. (b) Gordon, M. H.; Rico, R. J.; Oumi, M.; Lee, T. J. *Chem. Phys.Lett.* **1994**, *219*, 21. (c) Gordon, M. H.; Maurice, D.; Oumi, M. *Chem. Phys. Lett.* **1995**, *246*, 114.

(18) (a) Helgaker, T.; Jørgensen, P. *J. Chem. Phys.* **1991**, *95*, 2595. (b) Bak, K. L.; Jørgensen, P.; Helgaker, T.; Rund, K.; Jenson, H. J. A. *J. Chem. Phys.* **1993**, *98*, 8873. (c) Autschbach, J.; Ziegler, T.; Gisbergen, S. J. A.; Baerends, E. J. *J. Chem. Phys.* **2002**, *116*, 6930.

(19) (a) Cancès, E.; Mennucci, B.; Tomasi, J. *J. Chem. Phys.* **1997**, *107*, 3032. (b) Cossi, M.; Barone, V.; Mennucci, B.; Tomasi, J. *Chem. Phys. Lett.* **1998**, *286*, 253. (c) Mennucci, B.; Tomasi, J. *J. Chem. Phys.* **1997**, *106*, 5151.

(20) (a) Liu, T.; Zhang, H. X.; Xia, B. H. *J. Phys. Chem. A* **2007**, *111*, 8724. (b) Zhou, X.; Zhang, H. X.; Pan, Q. J.; Xia, B. H.; Tang, A. C. *J. Phys. Chem. A* **2005**, *109*, 8809. (c) Zhou, X.; Ren, A. M.; Feng, J. K. *J. Organomet. Chem.* **2005**, *690*, 338. (d) Albertino, A.; Garino, C.; Ghiani, S.; Gobetto, R.; Nervi, C.; Salassa, L.; Rosenverg, E.; Sharmin, A.; Viscardi, G.; Buscaino, R.; Cross, G.; Milanesio, M. *J. Organomet. Chem.* **2007**, *692*, 1377.

(21) Shi, L. L.; Liao, Y.; Zhao, L.; Su, Z. M.; Kan, Y. H.; Yang, G. C.; Yang, S. Y. *J. Organemet. Chem.* **2007**, *692*, 5368.

(22) (a) Hay, P. J.; Wadt, W. R. *J. Chem. Phys.* **1985**, *82*, 270. (b) Hay, P. J.; Wadt, W. R. *J. Chem. Phys.* **1985**, *82*, 299.

(23) (a) Machura, B.; Kruszynski, R.; Kusz, J. *Polyhedron* **2007**, *26*, 1590. (b) Machura, B.; Kruszynski, R. *J. Mol. Struct.* **2007**, *837*, 92.

(24) (a) Gabrielsson, A.; Matousek, P.; Towrie, M.; Hartl, F.; Záliš, S.; Vlček, A. *J. Phys. Chem. A* **2005**, *109*, 6147. (b) Dattelbaum, D. M.; Omberg, K. M.; Hay, P. J.; Gebhart, N. L.; Martin, R. L.; Schoonover, J. R.; Meyer, T. J. *J. Phys. Chem. A* **2004**, *108*, 3527. (c) Dattelbaum, D. M.; Martin, R. L.; Schoonover, J. R.; Meyer, T. J. *J. Phys. Chem. A* **2004**, *108*, 3518. (d) Lundin, N. J.; Walsh, P. J.; Howell, S. L.; McGarvey, J. J.; Blackman, A. G.; Gordon, K. C. *Inorg. Chem.* **2005**, *44*, 3551.

(25) Frisch, M. J.; Trucks, G. W.; Schlegel, H. B.; Scuseria, G. E.; Robb, M. A.; Cheeseman, J. R.; Montgomery, J. A., Jr.; Vreven, T.; Kudin, K. N.; Burant, J. C.; Millam, J. M.; Iyengar, S. S.; Tomasi, J.; Barone, V.; Mennucci, B.; Cossi, M.; Scalmani, G.; Rega, N.; Petersson, G. A.; Nakatsuji, H.; Hada, M.; Ehara, M.; Toyota, K.; Fukuda, R.; Hasegawa, J.; Ishida, M.; Nakajima, T.; Honda, Y.; Kitao, O.; Nakai, H.; Klene, M.; Li, X.; Knox, J. E. ; Hratchian, H. P.; Cross, J. B.; Adamo, C.; Jaramillo, J.; Gomperts, R.; Stratmann, R. E.; Yazyev, O.; Austin, A. J.; Cammi, R.; Pomelli, C. J.; Ochterski, W.; Ayala, P. Y.; Morokuma, K.; Voth, G. A.; Salvador, P.; Dannenberg, J. J.; Zakrzewski, V. G.; Dapprich, S.; Daniels, A. D.; Strain, M. C.; Farkas, O. D.; Malick, K. A.; Rabuck, D.; Raghavachari, K.; Foresman, J. B.; Ortiz, J. V.; Cui, Q.; Baboul, A. G.; Clifford, S.; Cioslowski, J.; Stefanov, B. B.; Liu, G.; Liashenko, A.; Piskorz, P.; Komaromi, I.; Martin, R. L.; Fox, D. J.; Keith, T.; Al-Laham, M. A.; Peng, C. Y.; Nanayakkara, A.; Hallacombe, M.; Gill,CP. M. W.; Johnson, B.; Chen, W.; Wong, M. W.; Gonzalez, C.; Pople, J. A. *Gaussian 03*, revision C.02; Gaussian, Inc.: Wallingford, CT, 2004.

(26) (a) Yang, L.; Ren, A. M.; Feng, J. K.; Liu, X. D.; Ma, Y. G.; Zhang, H. X. *Inorg. Chem.* **2004**, *43*, 5963. (b) Yang, L.; Ren, A. M.; Feng, J. K.; Liu, X. J.; Ma, Y. G.; Zhang, M.; Liu, X. D.; Chen, J. C.; Zhang, H. X. *J. Phys. Chem. A* **2004**, *108*, 6797.

(27) Ho, C. L.; Wong, Y. W.; Gao, Z. Q.; Chen, C. H.; Cheah, K. W.; Yao, B.; Xie, Z. Y.; Wang, W.; Ma, D. G.; Wang, L. X.; Yu, X. M.; Kwok, H. S.; Lin, Z. Y. *Adv. Funct. Mater.* **2008**, *18*, 319.

(28) Yang, L.; Feng, J. K.; Wong, W. Y.; Poon, S. Y. *Polymer* **2007**, *48*, 6457.

(29) Symcox, R. O.; Ehrlich, P. *J. Am. Chem. Soc.* **1962**, *84*, 531.

(30) Zhou, G. J.; Ho, C. L.; Wong, W. Y.; Wang, Q.; Ma, D. G.; Wang, L. X.; Lin, Z. Y. *Adv. Funct. Mater.* **2008**, *18*, 499.

(31) Yang, G. C.; Su, T.; Shi, S. Q.; Su, Z. M.; Zhang, H. Y.; Wang, Y. *J. Phys. Chem. A* **2007**, *111*, 2739.

(32) Hay, P. J. *J. Phys. Chem. A* **2002**, *106*, 1634.

(33) Zhou, G. J.; Ho, C. L.; Wong, W. Y.; Wang, Q.; Ma, D. G.; Wang, L. X.; Lin, Z. Y. *Adv. Funct. Mater.* **2008**, *18*, 499.

(34) Hush, R. A. *J. Chem. Phys.* **1958**, *28*, 962.

(35) Marcus, R. A. *J. Chem. Phys.* **1956**, *24*, 966.

(36) Marcus, R. A. *Rev. Mod. Phys.* **1993**, *65*, 599.

JP805758N